Methods for Atmospheric Correction in INSAR Data

Franz Meyer[1,2], **Bert Kampes**[1], **Richard Bamler**[1,2], **Juergen Fischer**[3]

[1] *Remote Sensing Technology Institute, German Aerospace Center (DLR)*
Oberpfaffenhofen, D-82234 Wessling, Germany
franz.meyer@bv.tum.de
[2] *Remote Sensing Technology, Technical University Munich*
Arcisstrasse 21, D-80333 Mnchen, Germany
[3] *Institute of Space Sciences, Free University Berlin*
Carl-Heinrich-Becker-Weg 6–10, D-12165 Berlin, Germany

ABSTRACT

Atmospheric effects are an important error source influencing the interpretation of interferometric products in terms of topography and displacement. These effects and several methods for correcting them in SAR and in InSAR data are currently investigated in the framework of the ESA Cat. I project ACID (Atmospheric Correction of InSAR Data). In this contribution, work in progress is reported, in particular related to the benefit of Kriging interpolation for separating atmospheric signal from noise for the application of Persistent Scatterer Interferometry (PSI). In addition, the use of MERIS data for mitigating atmospheric influences in interferometric ENVISAT ASAR data is investigated.

1 Introduction

A focused SAR image contains information on both, the backscattered amplitude and the two-way signal travel time between the radar antenna and the resolution cells on the ground. As the radar signal is traversing the earth's atmosphere twice, the signal path as well as the signal's propagation velocity is affected by the presence of the atmosphere. Several studies have shown that the predominant part of the atmospheric signal in interferometric products is caused by the water vapor distribution in the lower troposphere [Hanssen, 2001]. Depending on the air temperature and the air humidity, the one-way delay due to atmospheric water vapor can reach up to 21 cm (for $PWV = 3$ cm and $\theta_{inc} = 20°$), which corresponds to several phase cycles. Additionally, water vapor is characterized by a high spatial and temporal fluctuation. Hence, its influence on the phase of a focused SAR image or interferogram is highly unpredictable in space and time.

Several approaches for mitigating atmospheric effects in SAR interferograms have been proposed within the last years. Most of them use the spatio-temporal properties of water vapor for separating the atmospheric signal from other phase contributions. In this paper we propose to use Kriging interpolation for distinguishing between atmospheric contributions and noise in Persistent Scatterer Interferometry (PSI).

The sensor systems ASAR and MERIS on board of the ENVISAT satellite open up new possibilities in InSAR data processing. MERIS is capable to measure tropospheric water vapor with high spatial resolution and high accuracy. As both sensors are on the same platform, these observations are captured simultaneously. In this paper, the theoretical benefit of MERIS for InSAR applications and limitations of such an approach are described.

2 Theoretical covariance of the atmospheric phase screen

The atmospheric signal observed in a repeat pass SAR interferogram is governed by turbulent processes in the atmosphere, if sufficiently flat terrain is observed (topographic difference smaller than, say, 1 km). These turbulent processes cause heterogeneities in the refractive index during both SAR acquisitions used to generate the interferogram. The atmospheric signal in an SAR interferogram is expected to be a zero mean Gaussian processes with a standard deviation that depends on the weather conditions during the two acquisitions. The behavior of the atmospheric signal in the phase of radar interferograms can be mathematically described by measures like the *power spectrum*, the *covariance function*, the *structure function* and the fractal dimension [Hanssen, 2001].

Turbulent processes cascade down from large scales to smaller scales until the energy is dissipated. The spatial variation of the refractivity can be described by Kolmogorov turbulence theory, which assumes a specific structure function $D_N(\rho)$, depending on the distance ρ. This structure function predicts decorrelation of the refractivity with distance according to a $\rho^{2/3}$ law for distances smaller than 2 km, and an increased decorrelation for larger distances following a $\rho^{5/3}$

slope. Comparison of this theory with real data acquired during a variety of weather conditions show good correspondence. Figure 1 shows examples of a comparison of InSAR structure functions (bold lines) with the theoretical slopes (dashed lines).

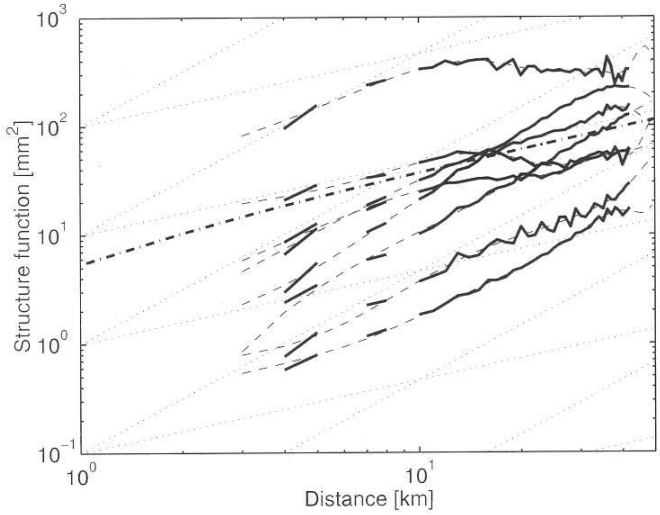

Figure 1: (Taken from [Hanssen, 2001].) Comparison of empirical structure functions (bold lines) of the tropospheric signal derived from ERS data with the theoretical model (dashed lines). Each line corresponds to a separate interferogram of the same area. Note that more severe weather conditions increase the power of the signal, but do not affect the slope of the structure function.

3 Separating atmospheric signal from noise in PSI

PSI allows to estimate topographic height and surface displacement at the persistent scatterers position with very high accuracy. The baseline dependence of the topography related phase ϕ_{topo} and the temporal dependence of the deformation phase ϕ_{defo} enables their separation from the remaining phase contributions, which are governed by a noise part ϕ_{noise} and the atmospheric phase screen ϕ_{atm}. If the real surface motion fits the used deformation model, the residual phase after subtracting the estimates can be written as:

$$\phi_{res} = \phi_{noise} + \phi_{atm} \tag{1}$$

By separating noise from atmosphere in Equation 1 the atmospheric condition during observation can be reconstructed and monitored. As the signal of both components is spectrally overlapping, distinguishing between noise and atmosphere is a non-trivial problem, and has already been treated in several publications. We propose to use Kriging interpolation to both separate atmosphere from noise and interpolate the atmosphere to a closed phase screen.

3.1 Kriging

Kriging is a regression technique used in geostatistics to approximate or interpolate data. Kriging can be understood as linear prediction or a form of Bayesian inference. It starts with a prior that takes the form of a Gaussian process: N samples from a function will be normally distributed, where the covariance between any two samples is the covariance function (or kernel) of the Gaussian process evaluated at the spatial location of two points.

Besides the prior, a set of observations, each associated with a spatial location, is needed as input information. Now, a new value can be predicted at any new spatial location, by combining the Gaussian prior with a Gaussian likelihood function for each of the observed values. The resulting posterior distribution is also a Gaussian, with a mean and covariance that can be computed from the observed values, their variance, and the kernel matrix derived from the prior.

The goal of Kriging is to obtain the conditional expectation as a best estimate for all unsampled locations in a field and consequently, a minimized error variance at each location. The conditional expectation minimizes the error variance when the optimality criterion is based on least squares residuals. The Kriging estimate is a weighted linear combination

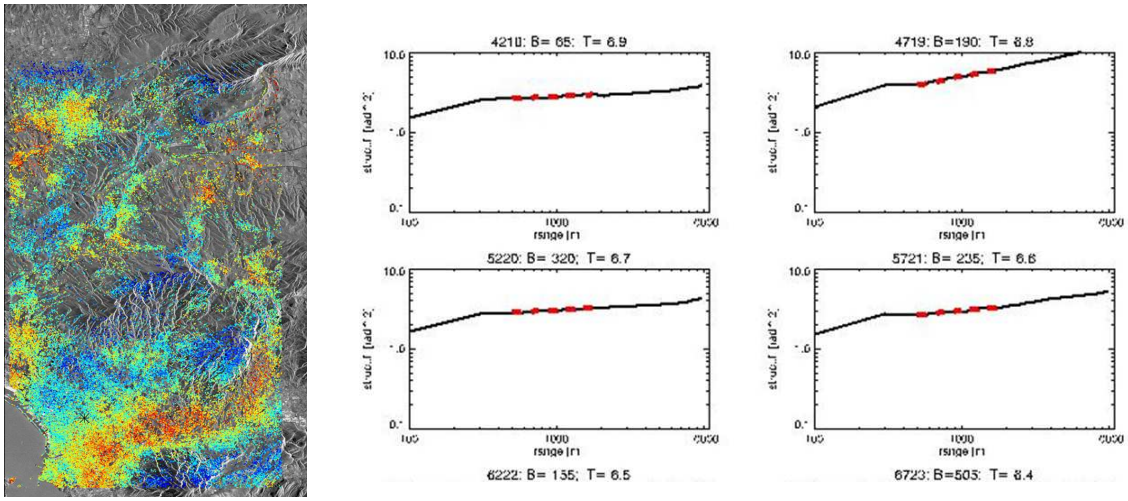

a) *b*)

Figure 2: a) Example of a residual phase screen after subtraction of the topography and displacement estimates. The example is taken from the PSIC4 study b) Structure Functions for 4 different residual phase screens. The red dashed line corresponds to estimates of the slope exponent of the structure functions. Note the logarithmic scale on both axes.

of the data. The weights are determined by solving the Kriging system of linear equations, where the weights are the unknown regression parameters. The optimization criterion used to arrive at the Kriging system, as mentioned above, is a minimization of the error variance in the least-squares sense. A detailed mathematical description of Kriging can be found in [Deutsch and Journel, 1998].

Thus, Kriging is the optimal method for the purpose at hand. Still, the a priori covariance function of the atmospheric phase screen has to be known. There are two ways to obtain this information: *i*) derive the covariance from theory of turbulent mixing; *ii*) estimate the covariance from real data.

3.2 Application of Kriging for atmospheric correction

In order to study whether or not reliable structure functions can be derived from real data we calculated structure functions of residual phase screens and compared them to their theoretical opponents $D_N(\rho)$. The area around Marseille was used as a test site. The data has been provided by ESA for the PSIC4 study and processed with PSI-GENESIS system [Kampes, 2006]. Figure 2*a*) shows a typical example for residual phase values of a single interferogram. Large scale phase fluctuations indicate atmospheric contributions. Four typical empirical structure functions are shown in Figure 2*b*) in a log-log scale, exemplified for the test data set. From the empirical structure functions the slope exponent is estimated using an exponential model for a range interval ranging from 500 m to 2000 m. The estimated slopes are indicated by the red dashed lines.

An analysis of the estimated slope values shows a bias towards smaller exponents, meaning that the decorrelation of the residual phase screens with distance is more pronounced than expected from theory. This slope bias results from the influence of white receiver noise on the estimated structure functions. Figure 3 shows the results of a simulation where atmospheric signal has been superimposed on white sensor noise. The structure function of the simulated atmospheric signal follows the theoretical $\rho^{2/3}$ law and is represented by a red line. Three different realizations of the atmospheric signal are presented, with increasing signal magnitude. The white noise is shown as a green line. The slope of the noise term is zero. The blue line shows the structure function of the mixed signal. By comparison of the three resulting structure functions, it can be easily seen that the slope bias is a function of the ratio between atmospheric signal and system noise and decreases with increasing signal-to-noise ratio. In the interferograms, the superposition of the noise and atmospheric signal is observed (blue line), and it is not possible to estimate the correct slope of the atmospheric signal without knowing the noise power.

This results suggests, that the covariance estimate derived from real data is biased depending on the signal-to-noise ratio. To come up with a more realistic covariance estimate, the biased measure needs to be corrected. However, if the correct covariance function is derived, Kriging interpolation is the method of choice for separating atmosphere from noise and for interpolating a full resolution atmospheric phase screen.

4 On the benefit of ENVISAT MERIS

ENVISAT is a multi-purpose earth-observation platform equipped with a wide range of instruments dedicated to monitoring our planet. Among them there is the Medium Resolution Imaging Spectrometer (MERIS), a multi-spectral camera, operating in the visible and near infrared part of the spectrum. Based on MERIS observations of reflected sun irradiance the integrated precipitable water vapor content (PWV) over cloud free land surfaces can be derived. The derivation method has been developed at the Institute of Space Sciences of the Free University Berlin and is described in more detail in [Fischer and Bennartz, 1997, Albert et al., 2001]. The quality of the MERIS water vapor product has been estimated and validated by comparison with Radio Sounding data [Albert et al., 2002], and GPS measurements [Li et al., 2003]. For comparison with radio sounding data the mean water vapor content of cloud free pixels within a 15 km radius has been calculated and compared to the radio sounding data. A standard deviation of $\sigma = 0.13\,gcm^{-2}$ and a bias of about $\mu = 0.05\,gcm^{-2}$ has been identified. Simultaneous GPS measurements confirmed this result. The intercomparison of GPS and MERIS resulted in a standard deviation of $\sigma = 0.17\,gcm^{-2}$ and a bias of $\mu = 0.02\,gcm^{-2}$. The results of the comparison with GPS data are shown in Figure 4. In both cases the standard deviation showed no pronounced dependency on the viewing angle of the MERIS sensor θ_{meris} and thus, on the position of the pixel in the MERIS scene. The Full Resolution Water Vapor Product of MERIS has a ground resolution of about 300×300 m.

4.1 Error propagation to the SAR phase

If precipitable water vapor is defined as

$$PWV = \frac{1}{\rho_l} \int \rho_v dh \tag{2}$$

where ρ_l is the density of liquid water $[10^6 gm^{-3}]$ and ρ_v is the density of water vapor, we can relate the precipitable water vapor to the slant delay $S_{k,v}^{t_i}$ for resolution cell k of a single SAR image acquired at time t_i using the equation of state $e = \rho R_v T$, as

$$S_{k,v}^{t_i} = \frac{1}{10^6 \cos\theta_{inc}} \rho_l R_v \left(k_2' + \frac{k_3}{T_m}\right) \frac{1}{\rho_l} \int \rho_v dh \tag{3}$$

with $R_v = 461.524\,[JK^{-1}kg^{-1}]$, and T_m is the mean temperature of the column containing the water vapor. Equation (3) holds if the contribution of liquid water to the phase of the SAR image can be ignored. The physical unit of pecipitable water vapor (PWV) is $[gm^{-2}]$ but it is usually given in $[mm]$. Equation (3) can be rewritten as

$$S_{k,v}^{t_i} = \frac{\rho_l R_v \left(k_2' + \frac{k_3}{T_m}\right)}{10^6 \cos\theta_{inc}} PWV = \frac{\Pi^{-1}}{\cos\theta_{inc}} PWV \tag{4}$$

where Π is a dimensionless factor of proportionality that maps zenith delay measurements on values of precipitable water vapor. Laboratory measurements of Π have been conducted by various scientists and a number of results are listed in literature. Usually, the result $\Pi \approx 0.15$ published in [Bevis et al., 1992, Bevis et al., 1996] is considered the most

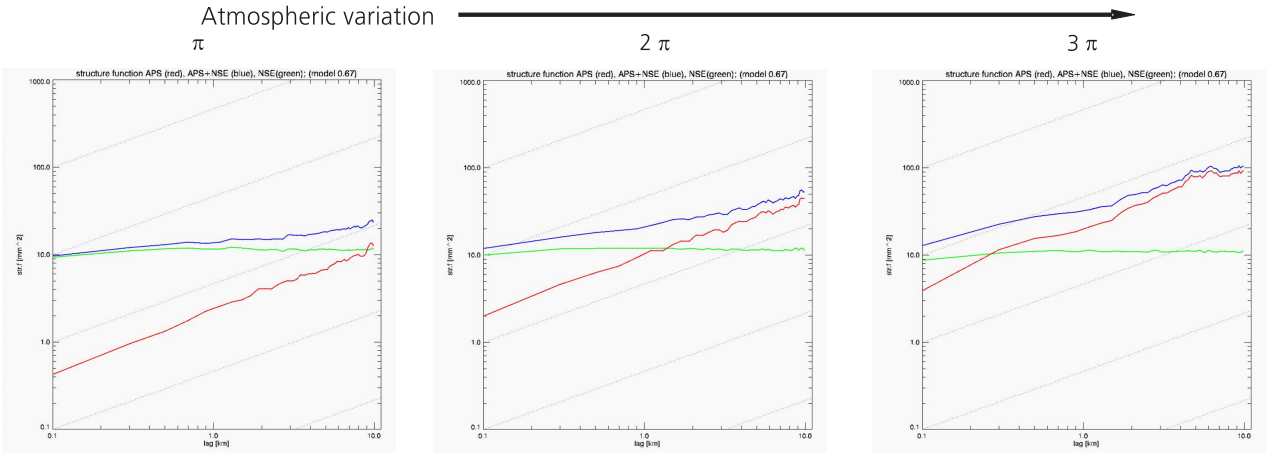

Figure 3: Change of the slope exponent of empirical structure functions dependent on signal magnitude and noise floor. The dependence of the slope change on the signal-to-noise ratio is clearly visible. Note the logarithmic scale on both axes.

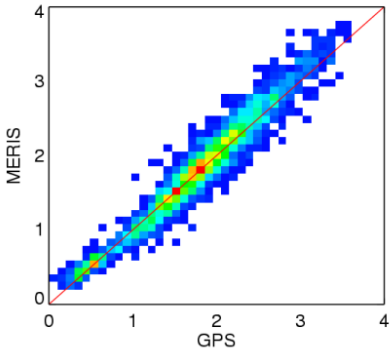

Figure 4: Scatter plot of columnar water vapor measured by GPS stations vs. MERIS estimates in g/cm2. Measurements are taken over Germany between October 2002 and September 2003.

reliable. In [Bevis et al., 1992] it is suggested that the proportionality factor is not constant but depends on the real surface temperature T_s at time and position of the measurement as well as on the geographic latitude of the test area. They give a linear regression for calculating the mean temperature T_m of the column containing the water vapor being

$$T_m \approx 70.2 + 0.72 \cdot T_s \tag{5}$$

According to [Bevis et al., 1992, Bevis et al., 1996] Π can be estimated with an error of less than 2 % using this linear regression.

Considering Equation 4 the error of a measured PWV values can be propagated to an error of a phase value in a SAR image by

$$\sigma_{\psi_{k,v}^{t_i}} = \frac{4\pi}{\lambda} \frac{\Pi^{-1}}{\cos\theta_{inc}} \sigma_{PWV} \tag{6}$$

Considering a typical parameter set of $\sigma_{PWV} = 1.7$ mm, $\theta_{inc} = 30°$, and $\Pi = 0.15$, the calculated standard deviation of the SAR phase is $\sigma_\psi = 2.9$ rad (about 0.46 phase cycles). Due to the high resolution of the MERIS Water Vapor Product of 300×300 m an averaging of 3×3 pixels can be done without loosing atmospheric signal. The standard deviation of the averaged phase results in $\sigma_{\bar{\psi}_{k,v}^{t_i}} = \frac{1}{3} \cdot \sigma_{\psi_{k,v}^{t_i}} = 0.97$ rad. A propagation of the error to the interferometric phase results in $\sigma_{\bar{\phi}_{k,v}^{t_i}} = \sqrt{2} \cdot \sigma_{\bar{\psi}_{k,v}^{t_i}} = 1.37$ rad. An averaging of the MERIS PWV over an area of 10×10 pixels would lead to a standard deviation of the corrected interferometric phase in the order of the noise level ($\sigma_{\bar{\phi}_{k,v}^{t_i}} = 0.41$ rad). As a trade-off the resolution of the MERIS product would be reduced to $3 \times 3\,\mathrm{km}^2$. It has to be considered in this context that ergodicity of the signal in a neighborhood of 10×10 pixels has to be guaranteed.

4.2 Analysis of the MERIS atmosphere

As the MERIS water vapor product contains high resolution information about the spatial distribution of water vapor in the troposphere, an analysis of this data allows to check its consistency with theory. Cloudless MERIS scene were selected out of the data base and tiled into image chips of $3 \times 3\,\mathrm{km}^2$ size. Structure Functions were calculated for each of this image chips and compared to the theoretical functions. Figure 5*a*) shows an example of a MERIS water vapor product acquired during cloudless conditions. The PWV values are given in cm unit. Figure 5*b*) shows four examples of structure functions, which are calculated for every image tile. The red dashed lines represent the slope values estimated from the data, while the black dashed lines indicate the theoretical exponents. A comparison between the theoretical and the empirical slopes shows quite good correspondence for most of the image chips. The $\rho^{5/3}$-law for large scale variations is well represented in most of the tiles. The exponent for small scale structures is usually too small when estimated from MERIS data. Again, this effect can be explained by the influence of the noise component in the MERIS water vapor product on the estimated structure functions. All in all, the intercomparison shows good correspondence between MERIS data and turbulence theory.

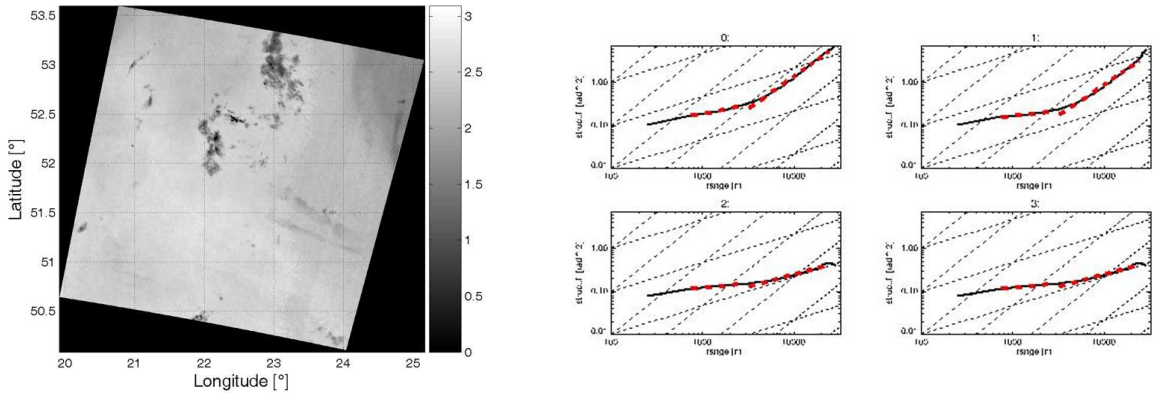

a) *b*)

Figure 5: a) Example of a full resolution MERIS water vapor product acquired during cloudless conditions. The PWV values are given in [cm]. b) Structure Functions for 4 different image tiled. The red dashed line corresponds to estimates of the slope exponent of the structure functions. The black dashed lines indicate the theoretical slope values. Note the logarithmic scale.

4.3 Pros and cons of MERIS

ENVISAT MERIS is a valuable tool to measure atmospheric water vapor on a global scale. The derivation approach is robust and accurate and allows to estimate precipitable water vapor with an accuracy sufficient for mitigating parts of the tropospheric influence in the phase of SAR images and SAR interferograms. However, the combined use of ENVISAT MERIS and ASAR has some major limitations.

As MERIS is a passive optical sensor, it is hampered by cloud coverage and is sensitive to illumination conditions. Especially in the area of central and eastern Europe, where the average sunshine duration is very low, cloudless data over your area of interest is hard to get. This is a severe limitation if periodical observations are necessary (e.g. in Persistent Scatterer Interferometry). As ASAR and MERIS observations must be acquired simultaneously, additional problems occur due to user conflicts.

Thus, combination of MERIS and ASAR for atmospheric correction is not a promising method if data should be acquired in a regular manner and independent on geographical location. Still, the sensor combination is very useful if data can be selected carefully and if areas with high sunshine duration are observed.

5 Conclusions

Since radar remote sensing has matured to a geodetic space technique that is capable to measure surface topography and surface motion with very high accuracy as well as high temporal and spatial resolution, studying the atmospheric influence on SAR and InSAR has become an important field of research. According to our investigations, Kriging is the optimal method to estimate atmosphere from the phase residuals of a PS stack. However, defining the a-priori covariance matrix is a problem that still has to be investigated in more detail. The MERIS water vapor product is an high-resolution and accurate measure for the precipitable water vapor in the troposphere. Combined with its simultaneous observation, it is a good tool to correct the phase of ASAR images for atmospheric contributions. Still, frequent cloud coverage over Europe and the illumination dependence of the MERIS sensor are severe limitations to the technique. The spatial properties of PWV measured by MERIS largely corresponds to theoretical considerations.

References

[Albert et al., 2001] Albert, P., Bennartz, R. and Fischer, J., 2001. Remote sensing of atmospheric water vapor from backscattered sunlight in cloudy atmospheres. Journal of Atmospheric and Oceanic Technology 18, pp. 865–874. 4

[Albert et al., 2002] Albert, P., Preusker, R. and Fischer, J., 2002. Verification of MERIS atmospheric level 2 products: Integrated water vapor above land, ocean and clouds. In: Envisat Validation Workshop, Frascati, ESA. 4

[Bevis et al., 1992] Bevis, M., Businger, S., Herring, T., Rocken, C., Anthes, R. and Ware, R., 1992. GPS meteorology: Remote sensing of atmospheric water vapor using the global possitioning system. Journal of Geophysical Research 97, pp. 15787–15801. 4.1, 4.1

[Bevis et al., 1996] Bevis, M., Chiswell, S., Businger, S., Herring, T. and Bock, Y., 1996. Estimating wet delays using numerical weather analysis and predictions. Radio Science 31(3), pp. 447–487. 4.1, 4.1

[Deutsch and Journel, 1998] Deutsch, C. and Journel, A., 1998. GSLIB - Geostatistical Software Library and User's Guide. Second edition edn, Oxford University Press, New York. 3.1

[Fischer and Bennartz, 1997] Fischer, J. and Bennartz, R., 1997. Retrieval of total water vapor content from MERIS measurements. Algorithm Theoretical Basis Document PO-NT-MEL-GS-005, ESA-ESTEC. 4

[Hanssen, 2001] Hanssen, R., 2001. Radar Interferometry: Data Interpretation and Error Analysis. Vol. 2, 1 edn, Kluwer Academic Publishers. 1, 2, 1

[Kampes, 2006] Kampes, B., 2006. Radar Interferometry: The Persistent Scatterer Technique. Remote Sensing and Digital Image Processing Series, first edition edn, Springer, New York. 3.2

[Li et al., 2003] Li, Z., Mueller, J., Cross, P., Hewison, T., Watson, R., Fischer, J. and Bennartz, R., 2003. Validation of MERIS near IR water vapor retrievals using MWR and GPS measurements. In: MERIS User Workshop, Frascati, ESA. 4